Journal of
Ship&Ocean
Technology
©JUNE 2008

SOTECH Vol. 12, No. 2, pp. 16 ~ 31, 2008

Unsteady Analysis of 3-Dimensional Hydrofoils Using a B-Spline Based High Order Panel Method

Hyun-Gil Jang[1], Byoung-Kwon Ahn[1] and Chang-Sup Lee[1]

[1] Department of Naval Architecture and Ocean Engineering, Chungnam National University, Chungnam, Korea;
Corresponding Author: csleepro@cnu.ac.kr

Abstract

The lifting-surface programs have been used successfully in practice for the design and global performance prediction of the marine propellers. To predict the pressures on the blade for the strength analysis, the constant panel method has been a good alternative. To meet the need for more accurate information on the pressure near the tip region and the trailing edge of the blade, the higher order panel method (HiPan, hereinafter) based on a B-spline is developed and now available. However, there is an increasing demand to get the highly reliable unsteady behavior of the pressure near the tip region by the HiPan. The ultimate goal of our efforts is to develop the fully unsteady higher order panel code for the propeller. In the present paper, we will show the numerical procedure applicable to unsteady problems of the three dimensional hydrofoil in a sinusoidal gust and heave motions.

Keywords: B-spline, higher-order panel method, hydrofoil, unsteady hydro-dynamics, gust, heave motions

1 Introduction

A large number of different panel methods have been developed and widely used in aerodynamic and hydro-dynamic designs, since the pioneering work of Hess and Smith (1964). Until Morino(1974) introduced a panel method based on Green's formula in which the primary unknown is the potential, most of the previous works were based on the velocity-based formulation in which the boundary condition on the body surface is satisfied through the direct computation of the velocity. Morino's potential-based formulation is known to be more stable and hence more suitable to numerical computation than the velocity method, since the potential is one order less singular than the velocity.

The existing potential-based methods are based on the low-order model in which the potential is constant over a panel and the velocity distribution on the body surface is calculated using a finite difference scheme. However, this method inevitably introduces a truncation error that is most significant near the trailing edge and the tip of the lift-generating surface, and results in degradation of the accuracy. Recently a B-spline based higher-order panel method (HiPan) has been developed and applied to the marine propeller analysis as an alternative way to reduce the error which is not recovered by lower-order

models. The order of B-splines to represent body geometries and potentials can be increased without limit, and hence solutions of any order can be obtained. The most detailed description of the higher-order panel method based on B-splines was first given by Hsin, Kerwin and Newman (1993) for the analysis of the flow around two-dimensional bodies.

Maniar (1995) extended it to three-dimensional cases. In his approach the integrals of the influence functions are expressed in terms of polynomials of a parametric coordinate, and the polynomial coefficients are derived from B-spline basis functions. Although the polynomial representation is sufficient for most bodies of interest, it is generally not appropriate to expand polynomials to non-uniform rational B-spline (NURBS) surfaces, which are the de-facto standard in industry to represent complex surfaces like ship hulls. Hong and Lee (1999 and 2002) applied the HiPan to the radiation problems of 2-dimensional floating bodies. Lee and Kerwin (2003) introduced a very general numerical procedure for the evaluation of influence coefficients for the analysis of lifting flows around two-dimensional and three-dimensional bodies including marine propellers. Lee and Kinnas (2005) presented an algorithm for the unsteady wake alignment based on a low-order panel method in which they applied the tip vortex core size using the method developed by Lee and Kinnas (2004). Instead of following Maniar's method, we adopt a conventional numerical integration method such as Gauss-Legendre quadrature. This approach is very simple mathematically and numerically, yet there is no loss in evaluating induction integrals accurately. The coding requires far less efforts than that of Maniar. Kim et al (2006 and 2007) successfully applied the HiPan to the analysis of the marine propellers and the radiation problem of floating bodies on the free surface. They considered a wake roll up model and showed improved results at tip regions of the propeller. Recently Park et al (2008) applied HiPan to the analysis of two dimensional unsteady hydrofoil problems.

In the present paper, we presented unsteady analysis of three dimensional hydrofoil problems such as gust and heave motions. This work is an intermediate stage to develop the fully unsteady higher order panel code for marine propellers.

2 B-spline representations

The potential is represented as a weighted sum of tensor product B-spline basis functions in a similar form as for the geometry as $\phi(u,v)$ along the surface of the body. However, instead of treating the potential directly, we represent the potential as a weighted sum of tensor product B-spline basis functions in a similar form as for the geometry:

$$\phi(u,v) = \sum_{i=0}^{N^v-1} \sum_{j=0}^{M^v-1} \phi_{i,j}^v N_i(u) M_j(v) \tag{1}$$

where $N_i(u)$ and $M_j(v)$ are the B-spline basis functions, $\phi_{i,j}^v$ the potential control vertices, and N^v and M^v the numbers of potential control vertices in u,v directions respectively. The numbers of potential control vertices (N^v, M^v) and the basis functions $(N_i(u), M_j(v))$ may be different from the corresponding quantities for the geometry, but usable parametric spaces of the geometry and potentials should be identical. With the introduction of the potential vertices, the unknowns of the hydrodynamic problem are now

values of the potential vertices $\phi^{v}_{i,j}$ that are not the potential in the physical sense. The potential knot vectors in (u,v) are defined:

$$\begin{aligned}\vec{U} &= \{0,0,0,0,1/N^{\phi},2/N^{\phi},\cdots,1,1,1,1,\}^{T}\\ \vec{V} &= \{0,0,0,0,1/M^{\phi},2/M^{\phi},\cdots,1,1,1,1\}^{T}\end{aligned} \tag{2}$$

The numbers of spans or panels in (u,v)-directions in usable parametric spaces for the potential are (N^{ϕ},M^{ϕ}) and they are related with the number of potential control vertices in forms of $N^{v}=N^{\phi}+p$ and $M^{v}=M^{\phi}+q$.

3 Discretized integral equation

The potential on the body surface is represented by the influences of the normal dipoles and the sources distributed on the body surface consisting of the body and the wake surface as

$$\frac{\phi}{2}=\iint_{S_B}\left[\frac{\partial\phi}{\partial\bar{n}}G-\phi\frac{\partial G}{\partial\bar{n}}\right]ds-\iint_{S_W}\Delta\phi\frac{\partial G}{\partial\bar{n}}dS \tag{3}$$

where ϕ is the perturbed velocity potential, $\bar{n}$ the unit normal vector of the body and wake surface, and G the Green function. Discretization into a set of (N^{ϕ},M^{ϕ}) panels on the body and M^{ϕ} strips in wake yields

$$\begin{aligned}&\frac{\phi}{2}+\sum_{\upsilon,\mu}\iint_{S_{\upsilon,\mu}}\phi\frac{\partial G}{\partial n}ds+\sum_{\mu}\iint_{S^{w}_{\mu}}(\Delta\phi)_{\mu}\frac{\partial G}{\partial n}ds\\ &=\sum_{\upsilon,\mu}\iint_{S_{\upsilon,\mu}}\frac{\partial\phi}{\partial n}GdS\end{aligned} \tag{4}$$

Noting that there are only $(p+1,\ q+1)$ nonzero basis functions at each span defined by the space between adjacent knots in (2), we may rewrite the potential (1) as a $(p+1,q+1)$ term summation:

$$\phi(u,v)=\sum_{a=0}^{p}\sum_{b=0}^{q}\phi^{v}_{\alpha,\beta}N_{\alpha}(u)M_{\beta}(v) \tag{5}$$

where subscripts (s,t) are span indices satisfying the relation $(u,v)\in((u_s,u_{s+1}),(v_t,v_{t+1}))$ in the knot vectors (2), $\alpha=s-p+a$ and $\beta=t-q+b$. Substitution of the equation (5) into (4) gives the control point on (i,j)-th panel:

$$\begin{aligned}
&\frac{1}{2}\{\sum_{a,b} N_{a_i}(u_i)M_{\beta_i}(v_i)\phi^{v}_{\alpha_i,\beta_i}\} \\
&+\sum_{\upsilon,\mu}\iint_{S_{\upsilon,\mu}}\{\sum_{a,b} N_{\alpha}(u)M_{\beta}(v)\phi^{v}_{\alpha,\beta}\}\frac{\partial G}{\partial n}dS \\
&+\sum_{\mu}\iint_{S^{w}_{\mu}}(\Delta\phi)_{\mu}\frac{\partial G}{\partial n}dS=\sum_{\upsilon,\mu}\iint_{S_{\upsilon,\mu}}\frac{\partial \phi}{\partial n}GdS
\end{aligned} \tag{6}$$

where $\alpha_i = s_i - p + a$, $\beta_i = t_i - q + b$, $\alpha = s_v - p + a$ and $\beta = t_\mu - q + b$. It should be noticed that the (υ,μ) summation for the dipole over the panels in (6) includes cases $i=\upsilon$ and $j=\mu$. In the low order panel method, these terms are eliminated, since the effect is already considered by the subtended angle of the hemisphere surrounding the point where the potential is evaluated. In the higher-order panel method, there are additional effects from the curvature of the geometry and the higher order variation of the potential in addition to the subtended angle effect.

4 De-singularized induction integrals

When the control point falls within the panel boundary, special care is necessary to avoid the singular behavior in computing the influence integral, especially when the coefficient of B-spline basis functions is constant in the equation (6). The induced potential due to the source and the dipole of constant strength are expressed respectively in the forms:

$$I_0^S = \frac{-1}{4\pi}\iint\frac{1}{r}dS \tag{7}$$

$$I_0^D = \frac{-1}{4\pi}\iint\frac{-\hat{n}\cdot\vec{r}}{r^3}dS \tag{8}$$

where the distance vector $\vec{r}$ is defined by a vector extending from the control point to the source point on the panel surface and is expressed by a series of B-spline tensor products as

$$\begin{aligned}
&\vec{r}=\sum_{a,b}(\vec{x}^{v}_{\alpha,\beta}-\vec{x}_c)\tilde{N}_{\alpha}(u)\tilde{M}_{\beta}(v) \\
&r=|\vec{r}|
\end{aligned} \tag{9}$$

The derivatives of the above with respect to the parametric variables can be obtained analytically from the B-spline derivatives as follows:

$$\begin{aligned}
&\frac{\partial\vec{r}}{\partial u}=\sum_{a,b}(\vec{x}^{v}_{\alpha,\beta}-\vec{x}_c)\frac{\partial\tilde{N}_{\alpha}(u)}{\partial u}\tilde{M}_{\beta}(v) \\
&\frac{\partial\vec{r}}{\partial v}=\sum_{a,b}(\vec{x}^{v}_{\alpha,\beta}-\vec{x}_c)\tilde{N}_{\alpha}(v)\frac{\partial\tilde{M}_{\beta}(v)}{\partial u}
\end{aligned} \tag{10}$$

With the partitioning, the integrals (7) and (8) are obtained by adding the contribution of each triangular section as

$$I_0^S = \sum_{k=0}^{3} I_{0,\Delta^{(k)}}^S = \sum_{k=0}^{3} \frac{-1}{4\pi} \int\int_{\Delta^{(k)}} \frac{1}{r} J d\xi d\eta \tag{11}$$

$$I_0^D = \sum_{k=0}^{3} I_{0,\Delta^{(k)}}^D = \sum_{k=0}^{3} \frac{-1}{4\pi} \int\int_{\Delta^{(k)}} \frac{-\hat{n}\cdot\vec{r}}{r^3} J d\xi d\eta \tag{12}$$

where J is the Jacobian of the surface element dS which is defined in the form;

$$J = \left| \frac{\partial \vec{r}}{\partial \xi} \times \frac{\partial \vec{r}}{\partial \eta} \right| \tag{13}$$

The unit normal vector to the surface element $\hat{n}$ can be computed by

$$\hat{n} = \frac{\partial \vec{r}}{\partial \xi} \times \frac{\partial \vec{r}}{\partial \eta} \Big/ J \tag{14}$$

Without loss of generality, we may describe the procedure to get the integral in the rightmost triangle $\Delta^{(0)}$ and this can be equally applicable to the other triangles. The quadratic transformation for $\Delta^{(0)}$ and their derivatives are

$$u - u_c = \xi \,, \qquad v - v_c = \xi\eta \tag{15}$$

$$\begin{aligned} \frac{\partial u}{\partial \xi} &= 1 \qquad \frac{\partial u}{\partial \eta} = 0 \\ \frac{\partial v}{\partial \xi} &= \eta \qquad \frac{\partial v}{\partial \eta} = \xi \end{aligned} \tag{16}$$

Maniar (1995) then showed that the distance vector $\vec{r}$ can be expressed by a product of the transform variable ξ and a finite nonzero vector quantity Q

$$\begin{aligned} \vec{r} &\equiv \xi \vec{Q}(u,v) \\ r &\equiv \xi Q(u,v) \end{aligned} \tag{17}$$

where $Q = \left|\vec{Q}\right|$ and ξ is non-negative within the triangle of transformation. This quantity (Q) is proportional to the ratio of the distance (r), between the collocation point and the singular point, and the coordinate ξ, and never becomes zero since ξ is factored out from $\vec{r}$ in (17). When the singular point falls on the ξ-axis and if the ξ variable is substituted by the curvilinear distance, the quantity Q will approach to unity, as shown by Lee and Kerwin (2003) for the 2-dimensional case. From the equation (17), we can also compute the vector normal to the surface element as

$$\frac{\partial \vec{r}}{\partial \xi} \times \frac{\partial \vec{r}}{\partial \eta} = \xi \left(\vec{Q} + \xi \frac{\partial \vec{Q}}{\partial \xi} \right) \times \frac{\partial \vec{Q}}{\partial \eta} \tag{18}$$

Substituting (17) and (18) into the source integral (11) for $\Delta^{(0)}$ yields

$$\begin{aligned} I^{S}_{0,\Delta^{(0)}} &= \frac{-1}{4\pi}\int\int_{\Delta^{(0)}} \left|\frac{\partial \vec{r}}{\partial \xi}\times\frac{\partial \vec{r}}{\partial \eta}\right| \frac{d\xi d\eta}{r} \\ &= \frac{-1}{4\pi}\int\int_{\Delta^{(0)}} \left|\left(\vec{Q}+\xi\frac{\partial \vec{Q}}{\partial \xi}\right)\times\frac{\partial \vec{Q}}{\partial \eta}\right| \frac{d\xi d\eta}{Q} \end{aligned} \tag{19}$$

where the integrand of the last expression is non-singular. Similarly, the quadratic transformation applied to the dipole integral for $\Delta^{(0)}$ gives

$$\begin{aligned} I^{D}_{0,\Delta^{(0)}} &= \frac{-1}{4\pi}\int\int_{\Delta^{(0)}} -\frac{\partial \vec{r}}{\partial \xi}\times\frac{\partial \vec{r}}{\partial \eta}\cdot\frac{\vec{r}}{r^3} d\xi d\eta \\ &= \frac{-1}{4\pi}\int\int_{\Delta^{(0)}} -\xi\left(\vec{Q}+\xi\frac{\partial \vec{Q}}{\partial \xi}\right)\times\frac{\partial \vec{Q}}{\partial \eta}\cdot\frac{\xi\vec{Q}}{|\xi|^3 Q^3} d\xi d\eta \\ &= \frac{-1}{4\pi}\int\int_{\Delta^{(0)}} \left\{\frac{-\vec{Q}\times\partial\vec{Q}/\partial\eta\cdot\vec{Q}}{\xi Q^3}\right. \\ &\qquad \left. -\left(\frac{\partial \vec{Q}}{\partial \xi}\times\frac{\partial \vec{Q}}{\partial \eta}\cdot\vec{Q}\right)\frac{1}{Q^3}\right\} d\xi d\eta \end{aligned} \tag{20}$$

The numerator of the first term in the integrand of the equation (20) is always zero, whereas the denominator is nonzero unless $\xi = 0$. We expect that this term will result in the solid angle of 2π, when the contributions from all four triangles are added together as described by Maniar(1995). This is the factor which leads to the $\phi/2$ term in the integral equation. With the nonzero denominator in the second term in the integral, we observe that the integrand is a regular function. The significance of the above expressions (19) and (20) is that the singular part is removed from the original equations (11) and (12), and hence we can apply a numerical quadrature to perform integrations. To compute the integrand of (20) using more familiar physical quantities rather than Q, we use the relation:

$$\begin{aligned} &-\left(\frac{\partial \vec{Q}}{\partial \xi}\times\frac{\partial \vec{Q}}{\partial \eta}\cdot\vec{Q}\right)\frac{1}{Q^3} \\ &= \frac{\partial \vec{r}}{\partial \xi}\times\frac{\partial \vec{r}}{\partial \eta}\cdot\frac{-\vec{r}}{r^3} + \frac{\vec{Q}\times\partial\vec{Q}/\partial\eta\cdot\vec{Q}}{\xi Q^3} \end{aligned} \tag{21}$$

All the variables in the first term in the right-hand side of (21) are well defined. The second term is identically zero, since $\xi \neq 0$ in our numerical integration for (20). Equations (19) and (20) may now be computed by applying Gauss-Legendre quadrature with global variables as follows

$$\begin{aligned} I^{S}_{0,\Delta^{(0)}} &= \frac{-1}{4\pi}\frac{\xi_R-\xi_L}{2}\frac{\eta_T-\eta_B}{2} \\ &\quad \sum_{m=0}^{M_g-1}\sum_{n=0}^{N_g-1} w_m w_n \left\{\left|\frac{\partial \vec{r}}{\partial \xi}\times\frac{\partial \vec{r}}{\partial \eta}\right|\frac{1}{r}\right\}_{n,m} \end{aligned} \tag{22}$$

$$I^D_{0,\Delta^{(0)}} = \frac{-1}{4\pi}\frac{\xi_R - \xi_L}{2}\frac{\eta_T - \eta_B}{2} \sum_{m=0}^{M_g-1}\sum_{n=0}^{N_g-1} w_m w_n \left\{ -\frac{\partial \vec{r}}{\partial \xi} \times \frac{\partial \vec{r}}{\partial \eta} \cdot \frac{\vec{r}}{r^3} \right\}_{n,m} \tag{23}$$

where ξ_L and ξ_R denote the ξ parameters at the control point and the rightmost side of the square, respectively, η_B and η_T the η parameters at the lower and upper ends of the square, respectively, w_n and w_m the weights of Gauss quadrature in ξ - and η -directions, and N_g and M_g the order of the Gauss quadrature in both directions, respectively. It will be shown later that the order of Gauss quadrature for the self-induction computation should be $(N_g)_{Self} \geq 4$ and $(M_g)_{Self} \geq 4$. Application of the similar equation to the other triangles of the square will complete the computation of the self-induced potentials due to the source and the dipole.

When the control point falls on the panel surface, the induction integral due to the normal dipole of higher order requires a special treatment as described above. The contribution of the higher orders is, however, less singular than that due to the constant term in dipole strength, and hence the same argument leading to (23) can be applied to evaluate the dipole-induced potential of higher-order as

$$\begin{aligned} I^D_{self} &= \sum_{k=0}^{3} I^D_{\Delta^{(k)}} \\ &= \sum_{k=0}^{3} \int\int_{\Delta^{(k)}} \phi \frac{\partial G}{\partial n} \\ &= \sum_{k=0}^{3} \int\int_{\Delta^{(k)}} \sum_{a,b} \phi^v_{\alpha,\beta} N_\alpha(u) M_\beta(v) \frac{\partial G}{\partial n} J d\xi d\eta \end{aligned} \tag{24}$$

Since the source strength $\partial\phi / \partial n$ in (4) is known from the kinematic boundary condition, the evaluation of the self-induction due to sources of higher order is rather straightforward. The self-induction integral due to sources can be evaluated by applying Gauss-Legendre quadrature as follows:

$$\begin{aligned} I^S_{self} &= \sum_{k=0}^{3} I^S_{\Delta^{(k)}} \\ &= \sum_{k=0}^{3} \int\int_{\Delta^{(k)}} \frac{\partial \phi}{\partial n} G dS \\ &= \sum_{k} \frac{-1}{4\pi}\frac{\xi_R - \xi_L}{2}\frac{\eta_T - \eta_B}{2} \sum_{m,n} w_m w_n \left(\frac{\partial \phi}{\partial n}\frac{1}{r} J \right)_{n,m} \end{aligned} \tag{25}$$

When the control point is away from the dipole panel, it is possible to apply the far-field approximation directly in parametric spaces.

$$
\begin{aligned}
I_{far}^{D} &= \sum_{\mu,\nu} \iint_{S_{\nu,\mu}} \phi \frac{\partial G}{\partial n} dS \\
&= \sum_{\mu,\nu} \iint_{S_{\nu,\mu}} \sum_{a,b} \phi_{\alpha,\beta}^{\nu} N_{\alpha}(u) M_{\beta}(v) \frac{\partial G}{\partial n} J du dv \\
&= \sum_{\mu,\nu,a,b} \phi_{\alpha,\beta}^{\nu} \left\{ \iint_{S_{\nu,\mu}} N_{\alpha}(u) M_{\beta}(v) \frac{\partial G}{\partial n} J du dv \right\} \\
&= \sum_{\mu,\nu,a,b} \phi_{\alpha,\beta}^{\nu} \left\{ \frac{u_R - u_L}{2} \frac{v_T - v_B}{2} \right. \\
&\quad \left. \sum_{m,n} w_m w_n \left(N_{\alpha}(u) M_{\beta}(v) \frac{\partial G}{\partial n} J \right)_{n,m} \right\}
\end{aligned}
\tag{26}
$$

where $J = \left| \partial \vec{r} / \partial u \times \partial \vec{r} / \partial v \right|$. Note the summations over μ and ν is substituted by (24) when the (i, j)-th control point falls upon the self panel, that is when $i = \nu$ and $j = \mu$.

When the control point is away from the source panel, the integrand is not singular, and hence partitioning into triangles is not necessary. Knowing the exact expression for the strength of the source from the boundary condition, we may directly compute the values required at the Gauss integration points. The source-induction integral for the far field point may be evaluated as follows:

$$
\begin{aligned}
I_{far}^{S} &= \sum_{\mu,\nu} \iint_{S_{\nu,\mu}} \frac{\partial \phi}{\partial n} G dS = \sum_{\mu,\nu} \iint_{S_{\nu,\mu}} \frac{\partial \phi}{\partial n} G J du dv \\
&= \sum_{\mu,\nu} \left\{ \frac{u_R - u_L}{2} \frac{v_T - v_B}{2} \sum_{m,n} w_m w_n \left(\frac{\partial \phi}{\partial n} G J \right)_{n,m} \right\}
\end{aligned}
\tag{27}
$$

Note the summations over μ and ν is substituted by (25) when the (i, j)-th control point falls upon the self panel, that is when $i = \nu$ and $j = \mu$.

The far-field approximations of (26) and (27) are valid when the field point in where the potential is wanted is not sufficiently far from the panel. In this case, the panel is subdivided into 4 or more sub-panels and the induction integrals may be evaluated for the sub-panels applying the far-field formulations.

5 Unsteady pressure Kutta condition

In the lifting problem of the potential flow, kinematic and dynamic Kutta conditions should be satisfied. In case of the steady state, Morino type Kutta condition in which the potential difference between upper and lower side on the trailing edge is unique is sufficient. However, in case of the unsteady state another Kutta condition is required, and we apply unsteady pressure Kutta condition representing that the pressure difference between upper and lower surface of the trailing edge is zero:

$$
\Delta C_P = (C_P)_{upper} - (C_P)_{lower} = 0 \tag{28}
$$

Using the Bernoulli's equation the pressure jump at the trailing edge is expressed in the form:

$$\Delta p_{TE} = -\rho\left(\frac{\partial \Delta\phi_{TE}}{\partial t}\right) - \frac{1}{2}\rho\left(V_t^+ - V_t^-\right)_{TE}\left(V_t^+ + V_t^-\right)_{TE} \tag{29}$$

We, here, adopt second order approximation for the potential on the trailing edge which can replace the equation (29) into the non-dimensional form:

$$\begin{aligned}\left(\Delta C_P\right)_{TE} &= \frac{\Delta p_{TE}}{\frac{1}{2}\rho U^2} \\ &= -2\left(\frac{\partial \Delta\phi_{TE}}{U^2 \partial t}\right) - \left(\frac{V_t^+}{U} - \frac{V_t^-}{U}\right)_{TE}\left(\frac{V_t^+}{U} + \frac{V_t^-}{U}\right)_{TE} \\ &\equiv \left(\Delta C_P\right)_A + \left(\Delta C_P\right)_C\end{aligned} \tag{30}$$

First (added mass) and second terms (circulation) of the equation (30) can be expressed as

$$\begin{aligned}\left(\Delta C_P\right)_A &= -\frac{\Delta\left(3\phi^{(t)} - 4\phi^{(t-1)} + \phi^{(t-2)}\right)_{TE}}{UcU\dfrac{\Delta t}{c}} \\ \left(\Delta C_P\right)_C &= -\left(\frac{V_t^+}{U} - \frac{V_t^-}{U}\right)_{TE}\left(\frac{V_t^+}{U} + \frac{V_t^-}{U}\right)_{TE}\end{aligned} \tag{31}$$

Substituting the equation (31) into (30) yields

$$\begin{aligned}&-\frac{3}{U\Delta t/c}\frac{1}{Uc}\left[\phi_{N-1}^v - \phi_0^v\right]^{(t)} - \left[\hat{t}_{TE}^+ \cdot \frac{\vec{U}_{TE}^+}{U} - \hat{t}_{TE}^- \cdot \frac{\vec{U}_{TE}^-}{U}\right]^{(t)} \\ &\left[\frac{1}{U}\sum_{a=0}^{p}\phi_{N^\phi-1+a}^v\left\{\frac{N'_{N^\phi-1+a}(u_{TE}^+)}{ds/du}\right\} + \frac{1}{U}\sum_{a=0}^{p}\phi_a^v\left\{\frac{N'_a(u_{TE}^-)}{ds/du}\right\}\right]^{(t)} \\ &= -\frac{4}{U\Delta t/c}\frac{1}{Uc}\left[\phi_{N-1}^v - \phi_0^v\right]^{(t-1)} + \frac{1}{U\Delta t/c}\frac{1}{Uc}\left[\phi_{N-1}^v - \phi_0^v\right]^{(t-2)} \\ &\quad + \left[\hat{t}_{TE}^+ \cdot \frac{\vec{U}_{TE}^+}{U} - \hat{t}_{TE}^- \cdot \frac{\vec{U}_{TE}^-}{U}\right]^{(t-1)}\left[\hat{t}_{TE}^+ \cdot \frac{\vec{U}_{TE}^+}{U} + \hat{t}_{TE}^- \cdot \frac{\vec{U}_{TE}^-}{U}\right]^{(t-1)}\end{aligned} \tag{32}$$

where, ϕ_{N-1} and ϕ_0 are potentials on the upper and lower trailing edge, and superscripts +, – note the upper and lower surface of the wake sheet respectively. In case of the unsteady state, the integral equation (3) can be expressed as

$$\begin{aligned}\frac{\phi}{2} &= \iint_{S_B}\left[\frac{\partial\phi}{\partial\bar{n}}G - \phi\frac{\partial G}{\partial\bar{n}}\right]ds \\ &\quad - \iint_{S_{W_0}}\Delta\phi\frac{\partial G}{\partial\bar{n}}dS - \sum_{i=1,j=1}^{N-1,M-1}\iint_{S_{W_{ij}}}\Delta\phi\frac{\partial G}{\partial\bar{n}}dS\end{aligned} \tag{33}$$

where, S_B is a body surface, S_{w0} and S_{wij} are span-wise panels connected the trailing edge and remains of the wake sheet respectively.

6 Results and discussions

In the present work, we consider two different unsteady cases, one is a sinusoidal gust and the other one simple harmonic heave motion defined respectively

$$\bar{V}_\infty = \left|\bar{U}_\infty\right| \hat{i} + A_g \sin(\omega t - kx)\hat{j} \tag{34}$$

$$\bar{V}_\infty = \left|\bar{U}_\infty\right| \hat{i} + A_h \omega \sin(\omega t)\hat{j} \tag{35}$$

where A_g and A_h are amplitudes of the gust and heave motion respectively, and k is the wave number of the gust, ω angular velocity which is calculated from the relationship with the reduced frequency K:

$$K = \frac{\omega c}{2\bar{U}_\infty} \tag{35}$$

Here K=0.5 is used for all cases in the wok. We disregarded the added mass term in (30) as the reduced frequency is relatively small then its effect is not significant.

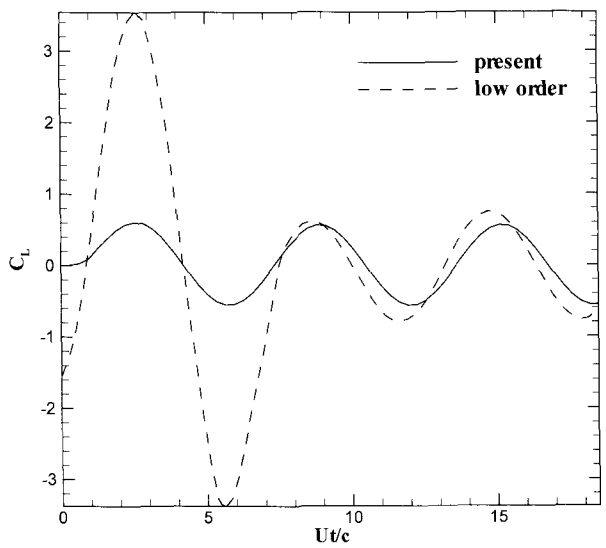

Figure 1: Comparison of the lift coefficient between the present and low order method (NACA0012 rectangular wing AR=5.0, α=0°, sinusoidal gust with A_g=0.2)

Figure 1 and 2 show lift coefficients of the rectangular wing (NACA0012, AR=5.0, α=0°) for a sinusoidal gust and a simple harmonic heave motion. Comparing with the low order panel method, the present gives quickly converged solution toward the harmonic steady state in both cases of the gust and heave motion. However, there are small

discrepancies in the phase between them and it is believed due to disregarding of the added mass term in (30) in the work. Figure 3 and 4 show lift and drag coefficients of the same wing and the same inflows with different amplitudes 0.01 and 0.2, which are relatively small and large. In both cases of the small amplitude, we can find leading edge suction force from drag coefficients.

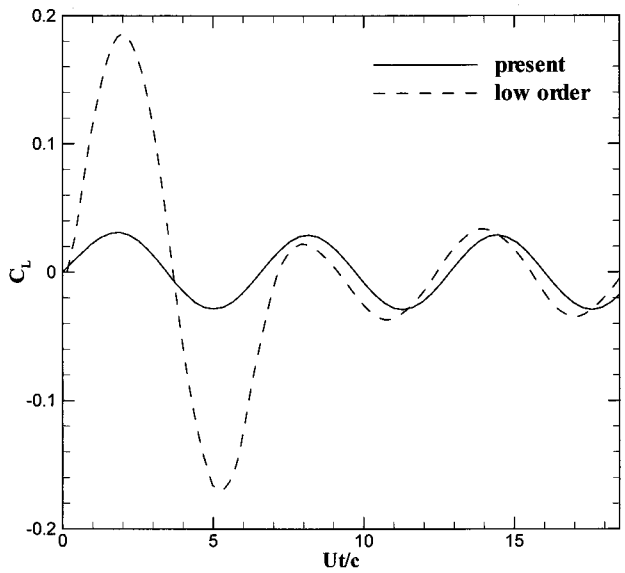

Figure 2: Comparison of the lift coefficient between the present and low order method (NACA0012 rectangular wing AR=5.0, α=0°, harmonic heave motion: A_h=0.2)

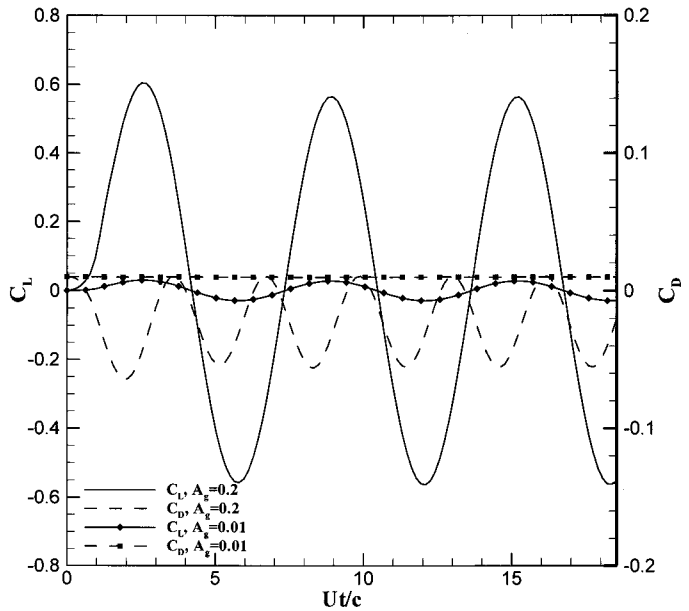

Figure 3: Lift and drag coefficients (sinusoidal gust: A_g=0.01 and 0.2)

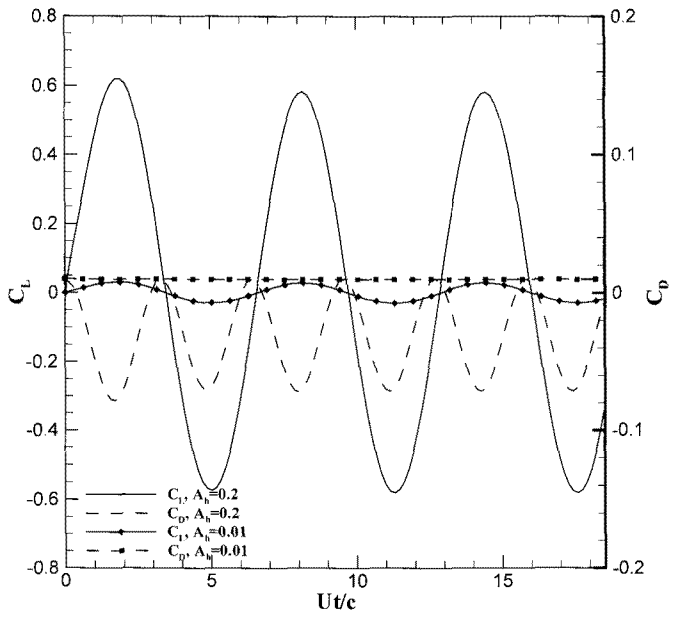

Figure 4: Lift and drag coefficients (harmonic heave motion: A_h=0.01 and 0.2)

Figure 5 and 6 show pressure distributions of span-wise direction for the same with previous cases. Solutions near tip region provide main advantage of the B-spline based high order panel method. In this region, numerous intricate flows appear and precise predictions are needed. As it mentioned previously, low order panel methods treat the potential as constant over a panel and it leads degradation of the accuracy which is relatively significant near the trailing edge. However, in the present method, the order of body geometries and potentials can be increased without limit and hence continuous solutions of any order can be obtained.

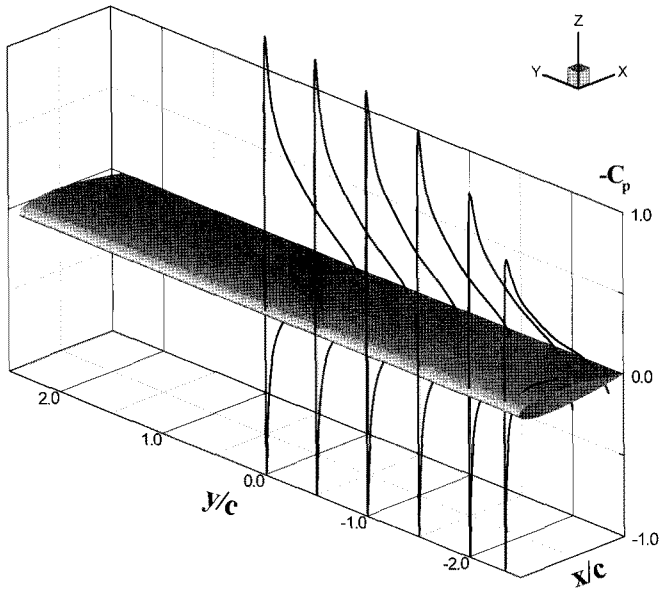

Figure 5: Pressure distributions (-Cp) of span-wise direction (sinusoidal gust: A_g=0.2)

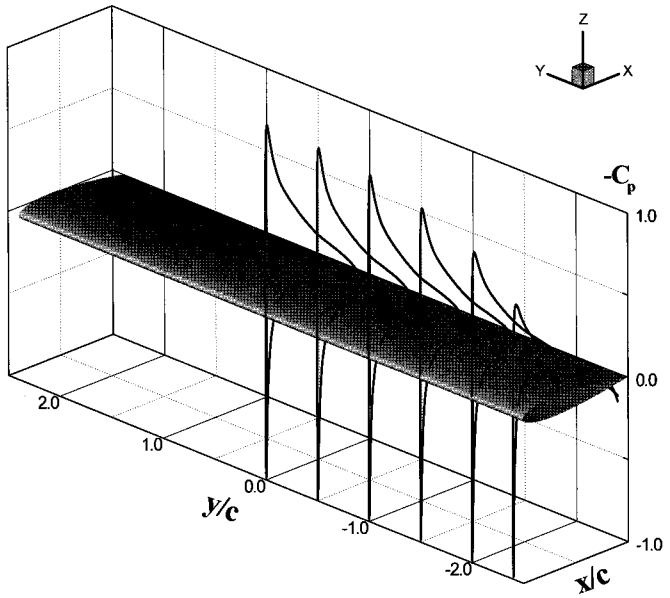

Figure 6: Pressure distributions (-Cp) of span-wise direction (harmonic heave motion: A_h=0.2)

Figure 7 and 8 show pressure coefficients at indicated time steps after two cycles for the same cases. In figure 9 and 10, circulations on the mid span (s=0.0) and both tip side strips (s=±2.5) are plot according to time differences. Circulation variances on the mid span strip give two dimensional information of the wing.

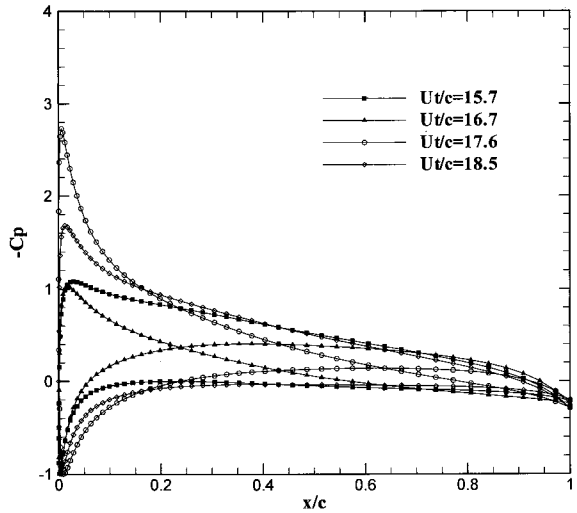

Figure 7: Pressure coefficients at Ut/c=15.7~18.5 (sinusoidal gust: A_g=0.2)

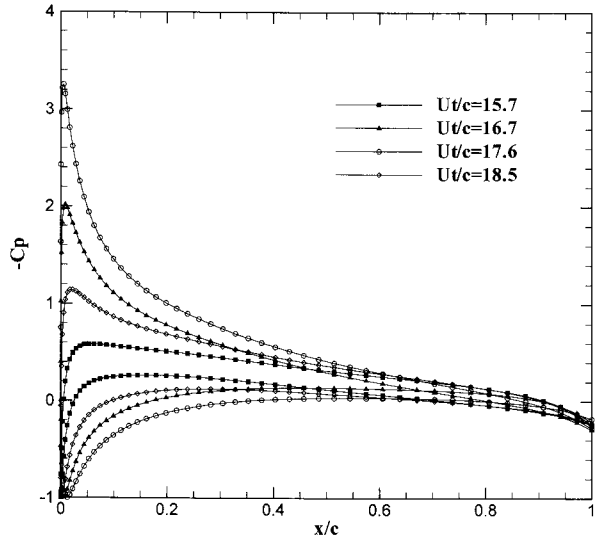

Figure 8: Pressure coefficients at Ut/c=15.7~18.5 (harmonic heave motion: A_h=0.2)

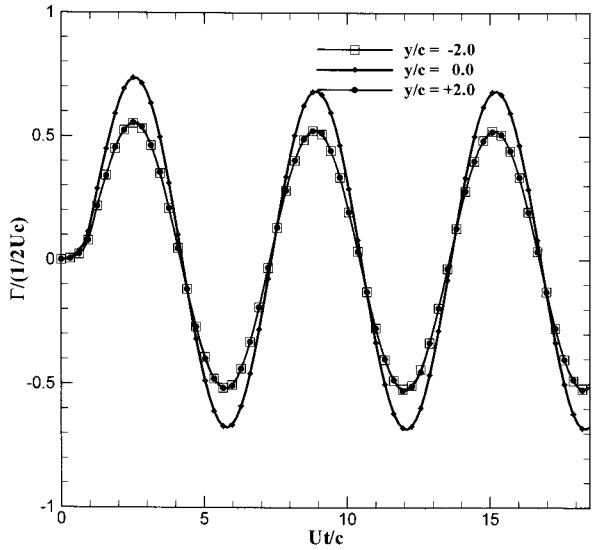

Figure 9: Circulation variance at different surface strips for a sinusoidal gust with Ag=0.2

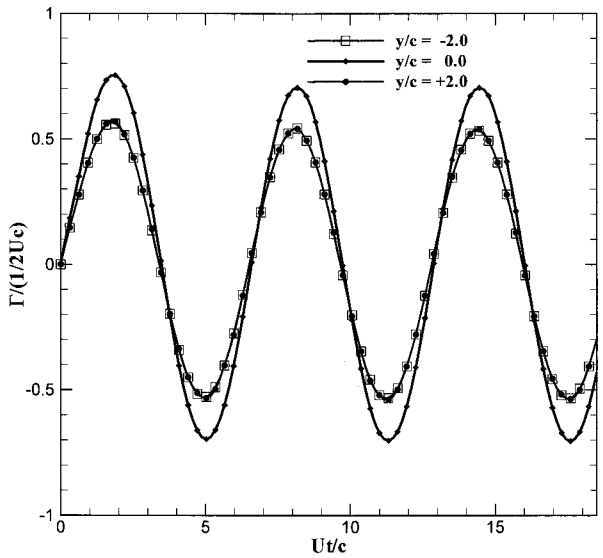

Figure 10: Circulation variance at different surface strips for a heave motion with Ah=0.2

7 Conclusions

Over the past few decades panel methods have been successfully used as a useful method in both practical aerodynamic and hydrodynamic designs. Recently a B-spline based higher-order panel method has been developed in demanding for more accurate information on the local flow likely the tip region and the trailing edge of the lifting body, and its steady state version is now available.

In the present work, we developed the numerical procedure which is applicable to three dimensional unsteady problems as an intermediate stage for the fully unsteady higher order panel code for the marine propeller. Two different unsteady cases of the three dimensional wing, sinusoidal gust and harmonic heave motion, were investigated. The results showed sufficient possibilities for applying this work to the corresponding problems of the marine propellers.

Acknowledgements

This work was carried out with the support of the Korea Science and Engineering Foundation (KOSEF) under Grant No. R01-2007-000-20376-0.

References

Hess, J.L. 1975. Review of Integral-Equation Techniques for Solving Potential-Flow Problems with Emphasis in the Surface-Source Method, Computational Methods in Applied Mechanics and Engineering, **5**, 145-196.

Hess, J.L. and A.M.O., Smith. 1964. Calculation of Nonlifting potential Flow About Arbitrary Three-Dimensional Bodies, Journal of Ship Research, **8**, **2**, 22-44.

Hess, J.L. and W.O. Valarezo. 1985. Calculation of Steady Flow about Propellers by Means of a Surface Panel Method, 23-rd Aerospace Science Meeting, AIAA, January 14-17, Reno, Nevada.

Hong, D.C. and C.S. Lee. 2002. Solution of the Radiation Problem by the B-Spline Higher Order Kelvin Panel Method for an Oscillating Cylinder Advancing in the Free Surface, Journal of Ship and Ocean Technology, **6**, **1**, 34-53.

Hong, D.C. and C.S. Lee. 1999. A B-Spline Higher Order Panel Method Applied to the Radiation Wave Problem for a 2-D Body Oscillating on the Free Surface, Journal of Ship and Ocean Technology, **3**, **4**, 1-14.

Hoshino, T. 1989. Hydrodynamic Analysis of Propellers in Steady Flow using a Surface Panel Method, Journal of the Society of Naval Architects of Japan, **165**, 55-70.

Hsin, C.-Y., J.E. Kerwin and J.N. Newman. 1993. HIPAN2: A Two-Dimensional Higher-Order panel Method Based on B-Splines, theory and program documentation, Department of Ocean Engineering, M.I.T.

Kim, G.D., B.K. Ahn, B.G. Paik, W.S. Lee and C.S. Lee. 2007. Numerical modeling of propeller tip flow with wake sheet roll-up by B-spline higher-order panel method, 10th International Symposium on Practical Design of Ship and Other-Floating Structures, **2**, 517-522.

Kim, G.D. and Lee, C.S. 2006 A 3-Dimensional Radiation Diffraction Problem Analysis by B-Spline Higher-Order Panel Method, Journal of Ship and Ocean Technology, Vol. 10, No. 1, pp. 10-26.

Kerwin, J.E., S.A, Kinnas, J.-T. Lee and W.-Z. Shih. 1987. A Surface Panel Method for the Hydrodynamic Analysis of Ducted Propellers, Transactions of SNAME, **95**, 93-122.

Lee, C.-S and J.E. Kerwin. 2003. A B-Spline Higher Order Panel Method Applied to Two-Dimensional Lifting Problem, Journal of Ship Research, **47**, **4**, 290-298.

Lee, H. and S.A. Kinnas. 2004. Application of BEM in the Prediction of Unsteady Blade Sheet and Developed Tip Vortex Cavitation on Marine Propellers, Journal of Ship Research, **48**, **1**, 15-30.

Lee, H. and S.A. Kinnas. 2005. Fully Unsteady Wake Alignment for Propellers in Non-axisymmetric Flows, Journal of Ship Research, **49**, **3**, 176-190.

Maniar, H.D. 1995. A three dimensional higher order panel method based on B-splines, PhD Thesis, Department of Ocean Engineering, M.I.T.